Comparison of a Microgel Simulation to Poisson-Boltzmann Theory [*]

Gil C. Claudio, Christian Holm, and Kurt Kremer

Max-Planck-Institut für Polymerforschung,

Ackermannweg 10, 55128 Mainz, Germany

Abstract

We have investigated a single charged microgel in aqueous solution with a combined simulational model and Poisson-Boltzmann theory. In the simulations we use a coarse-grained charged bead-spring model in a dielectric continuum, with explicit counterions and full electrostatic interactions under periodic and non-periodic boundary conditions. The Poisson-Boltzmann model is that of a single charged colloid confined to a spherical cell where the counterions are allowed to enter the uniformly charged sphere. We compare the simulational results to those of the Poisson-Boltzmann solution and find good agreement, i.e., for the number of confined counterions within the gel. We then proceed to investigate the origin of the differences between the results these two models give, and performed a variety of simulations which were designed to test for the influence of charge correlations, excluded volume interactions, and thermal fluctuations in the strands of the gel. Our results support the applicability of the Poisson-Boltzman cell model to study ionic properties of small microgels under dilute conditions.

I. INTRODUCTION

Hydrogel research has constantly attracted a lot of attention, due to its capability of absorbing large quantities of water, resulting in the expansion of the material up to 1000 times its dry volume. Recent review articles on hydrogel research range from general reviews[1] to application specific reviews such as sensors[2], surface applications[3], drug delivery applications[4] and other biomedical applications[5,6,7].

A hydrogel is a crosslinked network of water soluble polymers. The hydrophilicity of the free uncrosslinked chain allows it to attract water molecules and be soluble in water up to infinite dilution. The crosslinking, however, restricts the dilution to a maximal swelling of the gel. The combination of these two properties allows the hydrogel to attract water molecules and keep them within the network, resulting in an overall swelling of the entire gel. Hydrogels can be made of neutral or charged polymers called polyelectrolytes (the backbone of polyelectrolytes, however, need not be hydrophilic). When polyelectrolyte gels are dissolved in water, charges are formed in the polyelectrolyte when the counter ions dissociate from the polymer. These counter ions are free to move within the solvent, but stay, in the absence of salt, within the vicinity of the polyelectrolyte to keep electrostatic neutrality of the gel. The increase in entropy due to these counter ions overcomes the extra enthalpy to bring in even more water molecules into the network. The overall effect is that charged hydrogels have an even greater swelling ratio than their uncharged counterparts. A hydrogel matrix can be made to a few centimeters in diameter, depending on the synthetic procedure used. Microgels, on the other hand, are hydrogels that are within the micrometer range.

A number of analytical theories on hydrogels and polyelectrolytes have been presented[8,9,10,11,12]. Corresponding simulations have also been done[13,14,15], confirming the basic picture that the entropy of the counter ions exerts an extra osmotic pressure which in turn increases the swelling capacity of the hydrogels. Thus determining the location of these counter ions within the network, and specifically the investigation of ion condensation around the polymer chains, is an important aspect of hydrogel research. To our knowledge, the simulations that have been done, however, all consider quasi infinite systems via periodic boundary conditions that connect the chains of one side of the simulation box to its opposite side. This set up suffers from the limitation that the counter ions are, in a sense, always

inside the polymer matrix. Thus they cannot examine the actual charge fraction of counter ions inside the network which could, in turn, change the amount of osmotic pressure exerted by the counter ions, and thus change the swelling properties.

In an attempt to attack this problem, we simulate a model microgel, which is a finite sized object made up of crosslinked polymers in a periodic box. The simulation details are described in section II A. The system is a spherical polymer network in a simulation box, as shown in figure 1.

This model simulation allows us to calculate the counter ion condensation not only within the vicinity of each chain, but also the fraction inside the sphere, and study the consequences for the chain conformations. This model is also similar to an even more reduced model of a single charged sphere with counter ions that can be situated inside or oustide this charged sphere. This reduced model can be calculated using Poisson-Boltzmann (PB) theory. The simulation results can therefore be compared to a PB calculation, and thus provide evidence for the applicability of the Poisson-Boltzman cell model to study ionic properties of microgels.

There exists, however, quite a number of differences between the Poisson-Boltzmann method and simulation set-up, which can potentially confuse the interpretation of a direct comparison between the two. This paper examines the effects of these differences by presenting model simulations aimed at systematically removing, or adding, these factors in a step-wise fashion, with the final aim of studying the usefulness of the PB theory for a description of the swelling properties of microgels.

In section II, we describe the details of the microgel (MG) simulation (II A), brief description of PB theory (II B), and lastly the differences between PB calculation and the microgel simulation (II C). This list of differences (or assumptions) provides the rationale for the rest of the model simulations that we performed, aimed at connecting, in a stepwise manner, the PB model to the MG simulation. The methodologies and results of these simulations described in sections III through V. And in section VI, we give our counclusions.

II. MICROGEL SIMULATION AND POISSON-BOLTZMANN CALCULATION METHODOLOGIES

In all simulations, the following reduced units were used: energy is placed in terms of $k_B T$ which is given a value of 1.0, values of lengths are in σ, charge is in units of e, and time is in τ. All particles are given a mass of 1.0. Table I summarizes the parameters that are the same in all simulations in this paper, whereas table II and III lists the parameters that are specific to each simulation. All simulations were done using ESPResSo[16], a molecular dynamics package for soft matter simulations, under NVT conditions. In order to simulate a constant temperature ensemble, a Langevin thermostat is used, where all particles are coupled to a heat bath. Thus the equation of motion is modified to

$$m_i \frac{d^2 \vec{r}_i}{dt^2} = -\vec{\nabla}_i V_{tot} (\vec{r}_i) - m_i \Gamma \frac{d\vec{r}_i}{dt} + \vec{W}_i (t) \tag{1}$$

where m_i is the mass of particle i, V_{tot} is the total potential acting on the particle, Γ is the friction coefficient that is set to 1.0, and $\vec{W}_i(t)$ is a stochastic force that is uncorrelated in time and across particles. The friction and stochastic forces are linked by the fluctuation-dissipation theorem

$$\left\langle \vec{W}_i (t) \cdot \vec{W}_j (t) \right\rangle = 6m\Gamma k_B T \delta_{ij} \delta (t - t') \tag{2}$$

where $k_B T = 1.0$.

A. Microgel Simulation Details

The parameters for the microgel simulation are listed in Tables I and III, labelled as **P-MG**, where **P** indicates that periodic boundary conditions were used. Figure 1a shows how the starting structure of the microgel was constructed, whereas figure 1b gives a snapshot of an equilibrated microgel configuration. The microgel was simulated using a general bead-spring model[17,18]. The microgel was composed of 46 polymers, each composed of 10 monomers (beads), giving a total of 460 monomers. These polymers were connected by 29 crosslinks, each represented by one bead, giving a total of 489 beads (monomers plus crosslinks) in the microgel. Some crosslinks, especially those inside the microgel, were connected to the ends of four different polymers (serving as tetrafunctional nodes), while the rest were conneced to the ends of three different polymers (trifunctional nodes). Since all

of the polymer ends were connected to one crosslink, the microgel had no dangling chains. Upon examining figure 1a, one could see that the starting structure resembles that of a diamond lattice, with the edges cut off to approach a spherical shape. Once the particles are allowed to move, the average shape further approximates that of a sphere. The whole set-up was chosen to have an average equilibrated shperical shape, in order to make a comparison with the PB calculation of colloid using a cell model.

Half of the monomers (that is, 230) were given a charge of +1.0, while the others remained uncharged. The charged and uncharged monomers were placed along the polymer in an alternating sequence. Out of the 29 total crosslinks, 20 were also given a charge of +1.0, resulting to a total of 250 of the 489 total particles in the microgel having a charge of +1.0. Thus 250 free counter ions, each with a charge of -1.0, were added to the simulation, giving a total 739 objects and an overall neutral charge.

The non-bonded interactions of the particles were described by a Weeks-Chandler-Anderson potential[19] of the form

$$
U_{LJ}(r_{ij}) = \begin{cases} 4\epsilon_{LJ}\left[\left(\frac{\sigma_0}{r_{ij}}\right)^{12} - \left(\frac{\sigma_0}{r_{ij}}\right)^6 - c_{shift}\right] & \text{for } r_{ij} < r_{cut} \\ 0 & \text{for } r_{ij} \geq r_{cut} \end{cases}
\tag{3}
$$

where $\sigma_0 = 1.0$, $\epsilon_{LJ} = 1.0$, $r_{cut} = 2^{1/6}$, and $c_{shift} = 0.25$, thus leaving only the repulsive part of the interaction. These are the standard parameters for bead-spring model of polymers in a good solvent[19]. The bonds between the particles were modelled using the FENE (Finite Extension Nonlinear Elastic) potential[17]

$$
U_{FENE}(r) = \begin{cases} -\frac{1}{2}k_F r_F^2 \ln\left[1 - \left(\frac{r}{r_F}\right)^2\right] & \text{for } r < r_F \\ \infty & \text{for } r \geq r_F \end{cases}
\tag{4}
$$

where $k_F = 10.0\frac{k_B T}{\sigma^2}$ and $r_F = 1.5^{14}$. These parameters allow the bonds to equlibrate to $r \simeq 1.0$.

The potential energy between charges q_i and q_j separated by a distance r_{ij} were described by the unscreened Coulomb potential

$$
U_C(r_{ij}) = \frac{k_B T l_B q_i q_j}{r_{ij}}
\tag{5}
$$

where l_B, the Bjerrum length, is defined as

$$
l_B = \frac{e_0^2}{4\pi\epsilon_0\epsilon_r k_B T}
\tag{6}
$$

5

where e_0 is the elementary charge, ϵ_0 is the vacuum permittivity, and ϵ_r is the relative dielectric constant of the solvent. The Bjerrum length is defined as the distance at which the Coulomb energy between two unit charges is equal to the interaction energy of $k_B T$. This parameter provides a convenient way of tuning the strength of electrostatic interactions in a simulation. As a point of reference, the Bjerrum length of water at room temperature is 7.1 Å. In this paper, a Bjerrum length of $l_B = 1$ and $k_B T = 1$ was used in all simulations (Table I). Given a typical hydrogel such as poly(N-isopropylacrylamide) (poly-NIPAAm), the average distance between the centers of masses between two repeat units is within the order of 7.1 Å, making the choice of $r = 1.0$ and $l_B = 1.0$ both computational convenient and comparable to values of actual hydrogels.

The electrostatics for this simulation box was treated using the P3M algorithm[20,21], tuned to an accuracy of 10^{-4} in the absolute error of the Coulomb forces with the help of the formulas in Ref[21].

The MG simulation was performed in a cubic box with a length of 84 and periodic boundary conditions. This size was determined to be much larger than the Debye length of the system. The Debye length is the screening distance of a charged particle in a solution, beyond which its interaction with other ions is effectively screened. The Debye length is given as

$$\lambda_D = \frac{1}{\sqrt{8\pi l_B n_0}} \tag{7}$$

where n_0 is the molar conentration of ions in the reservoir, that is, the concentration of the counter ions remaining outside the sphere. As will be seen in the results, the microgel equilibrates to a radius of 15, with an average of 46% of the counter ions remaining outside the micorgel. This results to a Debye length of 14.1. The closest distance between two periodic images of the microgel is 54, which is roughly 3.8 times this Debye length. This method of calculating the molar concentration n_0 already yeilds the upper limit of the Debyle length. Choosing any other method for defining the n_0—for example, n_0 as the total number of counter ions over the total box volume—would yeild a higher value for n_0, and thus a shorter Debye length. This set-up therefore guarantees enough screening to prevent the microgel from being strongly electrostatically affected by its periodic image. Thus the microgel is in the dilute limit where each micgrogel behaves independently of other microgels. This allows us to compare the results with the PB calculations of a colloid in a cell model, which also assumes that the interaction of one colloid with other colloids is negligible.

B. Iterative Poisson-Boltzmann Solution

The Poisson-Boltzmann (PB) theory is a mean-field theory that describes the electrostatic interactions between charged particles in solution. The Poisson-Boltzmann equation is

$$\nabla^2 \phi\left(r\right) = -\frac{4\pi e_0}{\epsilon_0 \epsilon_r} \sum_i n_i^0 z_i \exp\left[-e_0 z_i \phi\left(r\right)/k_B T\right] \tag{8}$$

where $\phi(r)$ represents the electrostatic potential, and z_i is the valency of the ion species i. The charge density $\rho(r)$, assumed to be a Bolztmann distribution of charges, is given by

$$\rho\left(r\right) = -e_0 \sum_i n_i^0 z_i \exp\left[-e_0 z_i \phi\left(r\right)/k_B T\right] \tag{9}$$

This theory assumes that the only interactions taken into consideration are Coulombic interactions between point charges, thus neglecting any finite size effects of the charges. The other assumptions are that the ion entropy is that of an ideal gas.

In a cell model[22], one can approximate the interactions of a charged object with its counter ions in a local volume, and assume that the inteaction of this unit with other similar units is negligible. Using this model, we can therefore think of a microgel as one such charged object isolated in a spherical volume. This spherical cell model is shown in in figure 2a. The inner circle represents the charged object—for example, a colloid or a microgel—where the total (positive) charge of the object is distributed evenly within the sphere. This charged object has radius r_0. It is cocentric to an outer spherical cell of radius R, as represented by the outer circle in the figure. Counter ions are present in this spherical cell. In this study, these counter ions were represented as point charges with a charge of -1.0. They were allowed to go anywhere within the outer sphere, even into the charged object.

Our MG set-up (figures 1 and 2e) is fairly close to a charged sphere inside a spherical cell model (figure 2a). Solving the PB equation for this model of a charged sphere would therefore be a good comparison for the resulting distribution of charges of the MG simulation. The PB equation is a non-linear partial differential equation, and has closed-form analytical solutions only for a limited number of cases. For our case, it has to be solved numerically, as was done by Deserno et. al.[23,24], where the PB equation was solved numerically for the same spherical cell model as described above.

Using this PB numerical solver, we calculated the fraction of counter ions present in the charged sphere. The radius of the outer spherical cell was set to $R = 52$. The inner

charged sphere had a radius of $r_0 = 18$ and was given a total charge of $+250.0$. There were $n_{CI} = 250$ counter ions present, each with a charge of -1.0. The Bjerrum length was chosen to be $l_B = 1.0$. These parameters were chosen so as to match those of the MG simulation: the volume of the spherical cell is equal to the volume of the simulation box, and the charged sphere radius of $r_0 = 18$ is equal to the energy minimized structure (figure 2c) of the microgel coming from the initial structure (figure 1a). The parameters and results of this calculation, labelled as **PB-1**, are listed in Table II. The results will be discussed in the suceeding sections. One other PB calculation was done, labelled as **PB-2**, with slightly different parameters listed in III. The reason for this will be explained in the discussion of the MG simulation in section V.

C.   Rationale of the Simulation Strategy

The charged sphere in a cell model is already quite close to the microgel simulation. However, there still are quite a number of assumptions made between the PB model and the MG simulation. These are outlined as follows:

1. **Discrete Particles**. Whereas the total charge of the sphere in the PB model is uniformly distributed throughout the charged sphere, discrete charges are used in the MG simulation.

2. **Excluded Volume**. The microgel particles, whether charged or uncharged, in the MG simulation have excluded volume, as parameterized by σ_{LJ}, which in turn dertermines the local binding energy. This is non-existent in the charged sphere of the PB solver.

3. **Arranged Particles**. The charged particles in the MG simulation are situated along the chain, and are therefore not totally free to move relative to each other, differing from the even distribution of charges in the PB model.

4. **Thermal Fluctuations**. Aside from being arranged along the chains in the microgel, the charged particles also move as the polymer itself moves due to thermal fluctuations. This is not included in the PB theory.

5. **Periodic Boundary Conditions**. Lastly, the PB model was calculated in an isolated cell model, whereas the MG simulations were done under periodic boundary conditions.

This difference also compares the electrostatic algorithms employed in the two systems. When a simulation is done in a cell model, a direct sum of the Coulombic potential between all pairs of charged particles is calculated, whereas an Ewald sum approach— in this paper, the P3M algorithm—is done for the MG simulation in the periodic box.

Due to these assumptions, one would easily suspect that there would also be differences between the results of the PB calculation and the microgel simulation. However, it would be impossible to directly link the differences in results to each of these assumptions, since all of these assumptions are simultaneously present and could easily confuse the analysis. We therefore performed a series of model simulations that systematically remove from the original model one or more of the assumptions listed, thereby going from the PB picture to the MG simulation in a step-wise fashion. Using this procedure, we are able to attribute specific effects to the corresponding assumptions. These simulations are called Lattice Sphere (**C-LS**), Static Microgel (**C-ST**), and Microgel in a Sperical Shell (**C-MG**), which will be discussed below. The **C** in the labels indicate that they are done using a cell model, as compared to the microgel (**P-MG**), which was simulated using periodic boundary conditions (hence, labelled **P**). The set-ups of these simulations are shown in figure 2. The numbers on the arrows in this figure indicate the assumptions removed when going from one simulation to the next.

In all the calculations and simulations in this paper (as shown in figure 2), the following variables were kept constant:

1. **Total volume**. The total volume in which counter ions where free to move were the same for all simulations and **PB** calculations. An outer radius of $R = 52.0$ was used for all the calculations involving the spherical cell model. A cube with the same volume (within a 0.63% difference) has a length of $L = 84$, which is the value used for the simulations invovling a cubic box.

2. **Counter Ions**. The total number of counter ions was $n_{CI} = 250$, each with a charge of $q_{CI} = -1.0$.

3. **Charge of Inner Sphere**. In order to keep the system electrically neutral, the total charge of the inner sphere was kept at $q_{sp} = +250.0$. In some simulations, however,

the total number of charged particles in the inner sphere were greater than 250. In these cases, the fractional charge of these particles was adjusted in order to keep the total charge at +250.0.

III. LATTICE SPHERE SIMULATIONS (C-LS)

A. C-LS Methodology

We simulated a series of systems which we call Lattice Sphere (**C-LS**), which consist of charged particles that are fixed on a cubic grid. The set-up is shown in figure 2b. The final shape of this lattice approximates a sphere. This spherical lattice of radius $r_0 = 18$ was fixed at the center of an outer sphere with radius $R = 52$. Counter ions were placed inside the outer sphere. The outer sphere is given the same LJ repulsive term with parameters in Table I so as to keep the counter ions inside the sphere. During the simulation, the counter ions are free to move throughout the whole sphere (note that $R = 52$ is the radius of the volume available for counter ion motion). A repulsive Lennard-Jones potential was used between counter ions and the charged particles in the lattice so as to avoid that two oppositely charged particles to interact too strongly via Coulombic forces. No Lennard-Jones potential was used between counter ions, since these were treated as point particles, following the assumption of PB theory (section II B). This set-up is very similar to the PB model, except that two assumptions were already were lifted: discrete charged particles (assumption 1) distributed as evenly as possible within a sphere, and the added excluded volume (assumption 2) of these particles instead of an even charge distribution.

All **C-LS** simulations had a total of $n_{CI} = 250$ counter ions each with a charge of -1.0, and a total charge of $+250.0$ for the lattice. Given the various possible cubic lattice arrangements of charged particles with an overall spherical shape, the three arrangements used in this study had 250, 484 and 894 charged particles in the lattice sphere. And, in order for this sphere to retain a total of $+250$, charges of $+1.0$, $+0.516$, and $+0.279$, were distributed in these respective arrangments. In doing so, the point charges were systematically smeared out within the sphere, going from 250 ($+1.0$) to 484 ($+0.516$) and lastly to 894 ($+0.279$), therefore lessening the effect of charge discretization. In addition, the σ_{LJ} was also decreased from $\sigma = 1.0$ to smaller values. This has the effect of minimizing the effect

of excluded volume (assumption 2).

We used two ways of determining these smaller σ_{LJ} values. The first way was to maintain the energy of closest approach, that is, the Coulombic energy between the counter ion (with a charge of -1.0) and the charged particle (whether charged +1.0, +0.516, or +0.279) in the three different systems were always be the same. By examining equation 5, varying both the charge of the particle (q_i in the numerator) and the minimum distance (r_{ij} in the denominator) in the same way would yield equal energies. Thus, when varying the the charge from +1.0 to +0.516 to +0.279, we also varied the σ of the LJ potential in equation 3 from $\sigma = 1.0$ to $\sigma = 0.516$ to $\sigma = 0.279$. These are done in three calculations: **C-LS-1** with $\sigma = 1.0$, $q_i = +1.0$, and $n_{CP} = 250$; **C-LS-2** with $\sigma = 0.516$, $q_i = +0.516$ and $n_{CP} = 484$; and **C-LS-3** with $\sigma = 0.279$, $q_i = +0.279$ and $n_{CP} = 894$. Therefore the differences in results of these three calculations cannot be due to the energy of closest approach.

The second procedure used in decreasing the values of σ is by maintaining the ratio of the volume occupied by the charged particle to the volume of the entire inner sphere. In the previous procedure, the ratio of volumes of the charge particle to the inner sphere were 1.68×10^{-3} for **C-LS-1**, 4.44×10^{-4} for **C-LS-2**, and 1.30×10^{-4} for **C-LS-3**. Keeping this ratio equal to **C-LS-1**, the σ_{LJ} was changed to the following values for a new set of calculations: **C-LS-4** with $\sigma_{LJ} = 0.802$, $q_i = +0.516$ and $n_{CP} = 484$; and **C-LS-5** with $\sigma_{LJ} = 0.654$, $q_i = +0.279$, and $n_{CP} = 894$. Thus having kept the free volume inside the inner sphere constant, we can safely assume that the differences in results of these three calculations would not be due to entropic effects, which have been significantly reduced in this procedure.

These five Lattice Sphere simulations aimed at isolating the effects of the first two PB assumptions. The parameters and results are summarized in table II. These simulations were all done in a spherical cell model, with the electrostatics potential computed as a direct sum of Coulombic energies between all pairs of particles.

B.   Discussion: Result of Charge Discretization and Excluded Volume

Refering to table II, the first discussion compares the results of **PB-1**, **C-LS-1**, **C-LS-2**, and **C-LS-3**. These four calculations have the following parameters that are the same: total charge of sphere, number of counter ions, radius of charged sphere/lattice, and outer radius.

From calculations **C-LS-1** to **C-LS-2** to **C-LS-3**, the total number of discrete charged particles in the inner sphere was increased from 250 to 484 to 894, with a corresponding decrease in partial charge and σ_{LJ} from 1.0 to 0.517 to 0.279. Figure 3 shows the integrated counter ion probability of the simulations listed in Table II. The second to the last line in Table II refer to the results of the percentage counter ion in figure 3 where r is equal to the sphere radius r_0. The dots in the inset of figure 3 at $r_0 = 18\sigma$ indicate these percentages. Figure 4 shows the density of the counter ions as a function of the distance from the center of the inner sphere.

In general, the integrated counter ion probability (Fig. 3) and the counter ion density (Fig. 4) graphs of the **C-LS** simulations are close to the **PB-1** graph, with **C-LS-1** being the farthest and lower and **PB-1**, **C-LS-2** being closer but higher than **PB-1**, and **C-LS-3** being practically the same as the **PB-1**. The fraction of counter ions inside the sphere at $r_0 = 18$ (last line of Table II and the inset in Figure 3) also reflects this trend. As the number of charged particles is increased (with the corresponding decrease in partial charge) and thus the model becoming closer to the PB picture, the result of counter ion distribution approaches the PB calculation. Of the three LS calculations, the one with a unit charge of $+1.0$ can be considered closest of real physical systems, since charged particles always have unit charges. Thus we can say that the discretization of charges in a real system would have a counter ion condensation around 3% lower than what is predicted by PB theory.

However, there seems to be a slight anomaly in the trend shown above. Although a stepwise smearing out of the charges should have corresponded to a gradual approach to the **PB-1** calculation (52.83%), the results showed a jump from the lower value for **C-LS-1** (49.80%), to higher for **C-LS-2** (53.85%), then back down to practically equal for **C-LS-3** (52.78%) to the **PB-1** calculation. This trend cannot be caused by the energy of closest approach, since this has been set-up to be equal in these three LS calculations. We then proceed to examining the second assumption applied to the LS calculations, that of the excluded volume of the charged particles. The three calculations whose exculded volume, as measured by the ratio of volumes of charge particle to that of the inner sphere, are **C-LS-1**, **C-LS-4**, and **C-LS-5**. The integrated counter ion distribution and the counter ion densities of **C-LS-2** and **C-LS-4** are practically the same. The same is true for the graphs of **C-LS-3** and **C-LS-5**. The percentage of counter ions inside the inner sphere are listed at the bottom of table II. The trends are the same as the first set of LS calculations: **C-LS-1** is lower

(49.80%) than **PB-1** (52.83%), **C-LS-4** is higher (53.35%), and **C-LS-5** (52.23%) is closest to **PB-1**. This shows that the counter ion distributions is not dependent on the excluded volume of the charged particles.

The explanation of this trend simply comes from the ground state energies of the different set-ups, since the ground-state structures depend mainly on the configuration of the system. To do this, we set the Langevin temperature $T = 0.0$ and using a small friction coefficient Γ between 0.01 to 0.001 to allow for slow relaxation to the ground state. This resulting trend of the ground state electrostatic energies of these systems are similar to the trends in percentage counter ion in the sphere: **C-LS-1** being the highest $-2160.72k_BT$ (least stable), **C-LS-2** being the highest $-2301.29k_BT$ (most stable), and **C-LS-3** in the middle $-2293.17k_BT$. Thus the trend in counter ion fraction in the lattice sphere depends mostly on ground state configurations rather than the excluded volume of the charged particles. This does not mean, however, that excluded volume will not have an effect in polymeric systems. The next section discusses the more realistic arrangement of charged particles within a polymer chain.

IV.   STATIC MICROGEL SIMULATION DETAILS (C-ST)

A.   C-ST Methodology

After having seen the effects of assumptions 1 and 2, we then proceeded to simulate another system with assumption 3 removed, that of charged particles in the system being placed along the chains in the microgel. In this case, we took the coordinates of an expanded microgel with the same parameters as described in II A and fixed their coordinates so as not to allow thermal fluctuations. A snapshot of this system is shown in Figure 2c. This simulation is labelled as **C-ST**. Two versions of this simulation were performed. In the first case (**C-ST-1**), we removed the uncharged monomers (total of 230) so as not to include the effects of their excluded volume in the simulation. In the second case (**C-ST-2**), the uncharged monomers were not removed, so that the microgel has the same number of charged and uncharged particles present in the microgel simulations (**C-MG** and **P-MG**). These two therefore tested the effect of the arranging the charged particles along a chain, with the second looking at the added effect of the excluded volume of the uncharged particles, which

is therefore one step closer to the MG set-up. The parameters are similar to **PB** and **C-LS**, as listed in Table II. This particular arrangement of the particles had an overall effect of lessening the space between the charged particles beside each other on the same chain, and increasing empty spaces between charged particles on different chains. As with the Lattice Sphere case, this simulation was also done in a spherical cell model, with the electrostatics calculated as a direct sum.

B.   Discussion: Arrangement of Excluded Volume along a Polymer

The parameters and results of the static microgel simulations, **C-ST-1** and **C-ST-2**, are listed in Table II, with the integrated counter ion probability curve shown in figure 3 and the counter ion density shown in figure 4. The results show a further decrease of the fraction of counter ions in the static microgel **C-ST-1** (46.28%) and in **C-ST-2** (45.67%) as compared to **PB-1** (52.83%) and **C-LS-1** (49.80%). Figure 5 shows the relative distances of particles for the calculations of: a) **C-LS-1**, b) **C-ST-1**, and c) **C-ST-2**. The black circles represent the charged particles in the lattice sphere or microgel, the grey circle in fig. 5c represents the uncharged particle in **C-ST-2**, the dotted circles represent the excluded volume of these particles σ_{LJ}, and the unshaded circles represent the counter ions.

In the case of the **C-LS-1** configurations (fig. 5a), there is enough space in between two charged particles for a counter ions to move around the charged particle. The closest distance between the two dotted circles (given by x) is greater than 1.0, which is the Bjerrum length in the simulation. Thus even in this case, their Coulombic repulsion would still be much less than their thermal energy.

That is not the case for the static microgel (**C-ST-1**, fig. 5b) which does not include the uncharged particles in the microgel. The closest distance between paths (dotted circles) of two counter ions of adjacent charged particles is less than the Bjerrum length. Thus, unlike the lattice sphere cases, the space right in between two charged particles cannot be occupied by two counter ions, thus lessening the overall free space available for the counter ions. This effect could in turn decrease the fraction of charges in the microgel. The results of the second static microgel simulation (**C-ST-2**, fig. 5c) further supports this point. In this case, the additional uncharged particle (grey circle) contributes the extra excluded volume to the same space where electrostatic interactions prevented the counter ions to go, as argued

in the case of **C-ST-1**. Unlike the 3.52% drop from **C-LS-1** to **C-ST-1**, these two static microgel simulations have very close percentages of counter ions inside the gel—46.28% for **C-ST-1** and 45.67% for **C-ST-2**—indicating that the additional uncharged particles contributed only slightly to the reduction of counter ions in the gel. Thus the proximity of the charged particles in **C-ST-1** arranged along the polymers in the static microgel provided enough counter ion repulsion to lessen the avaialble space for counter ion motion and thus decrease the overall counter ion percentage in the sphere going from the **C-LS** to the **C-ST** calculations.

Although excluded volume had no effect on the configuration of the lattice sphere simulations as described in section III B, the specific arrangement of the excluded volume, in this case, arranged in a polymer chain, can slightly lessen the available space for counter ion condensation and thus lower the fraction of counter ions inside the microgel.

V. MICROGEL IN A SPHERICAL CELL (C-MG) AND IN A PERIODIC BOX (P-MG)

A. C-MG and P-MG Methodology

After removing assumptions 1 and 2 to the lattice sphere (**C-LS**) and assumption 3 to the static micro gel (**C-ST**), we then removed the next assumption 4, which looks at the effect of thermal fluctuations of the charged particles in the polymer. This is basically a microgel simulation, where the particles of the microgel are allowed to move, inside a spherical cell. Only the central particle of the microgel was kept fixed so as to keep the microgel in the center of the sphere. The parameters are basically the same as those of the microgel, and are listed in Table II. Aside from thermal fluctuations, the other difference of between this system and static microgel in a sphere (section IV) is the decrease in microgel radius, thus decreasing the free volume in between the chains. The parameters are listed in Table II. This simulation is labeled **C-MG**. As with the **C-LS** and **C-ST** simulations, the **C-MG** simulation was also done in a spherical cell model, with the electrostatics calculated as a direct sum.

To determine the effect of the last assumtion, that of periodic boundary conditions and differences in electrostatic algorithm, we compared the results of **C-MG** to **P-MG**. The

methodology and parameters for the **P-MG** simulation has already been discussed in section II A.

Due to the thermal fluctuation of the entire microgel for both **C-MG** and **P-MG**, the radius of the microgel was also fluctuating, but generally maintaing its overall spherical shape. In order to determine the average radius of the microgel, we used the following equation[25] that relates the square radius of gyration of a rigid sphere to the radius of the sphere

$$R_g^2 = \frac{3}{5}r^2 \tag{10}$$

where R_g^2 is square radius of gyration of the sphere with radius r.

B.   Discussion: Thermal Fluctuations and Periodic Boundary Conditions

The parameters and results (second to the last line) of the **C-MG** and **P-MG** are listed in Table III. The integrated counter ion probability is shown in figure 3 and the counter ion density is shown in figure 4. Allowing the microgel particles to move allowed the microgel shrink from $r_0 = 18$ for the static microgel simulation (**C-ST-1**) to an average of $r_0 = 14.96$ for **C-MG** and $r_0 = 14.99$ for **P-MG**. However, the fraction of counter ions within these radii for each simulation increased to 54.03% for **C-MG** and 53.95% for **P-MG**. Due to the difference of radius between **PB-1** and these two microgel simulations, another PB calculation,**PB-2** was done with a radius of $r_0 = 14.96$. The corresponding fraction of counter ions in the inner sphere for **PB-2** also increased to 55.59%, resulting in a decrease of 2.6% when going from PB calculation to MG simulation of the same radius r_0. As already seen in the discussion of the LS results in section III B, the simluation results correspond to the PB calculation, with a slight decrease of a similar value (3.0%) in the fraction of counter ions in the lattice sphere. This shows that the thermal fluctuations of charged particles in a polymer do not affect the counter ion fraction inside the MG.

The decrease of the radius of the charged microgel/sphere leads to an increase in fraction of counter ions in the micogel/sphere. This can be explained as follows. The decrease of the microgel/sphere radius, while keeping the total charge constant, corresponds to an increase in the overall charge density within the sphere, thus attracting more counter ions into the sphere. Our results of the PB calculations show that the gain in energy outweighs the loss of entropy, which the confined confined counter ions experience.

Both **C-MG** and **P-MG** have practically the same results—configuration as measured by R_g^2, fraction of counter ion inside the microgel, integrated counter ion probability (firgure 3) and counter ion densities (figure 4). Thus the spherical cell model simulation, whose electrostatics is calculated as a direct sum, is equivalent to the corresponding simulation under periodic conditions, as long as the sytsems are set up correctly. This means that the system size is done ensuring enough electrostatic screening (as calculated by the Debye length) in order to satisfy the "isolated system" assumption of the cell model, and that the P3M electrostatics is tuned correctly.

VI. CONCLUSIONS

We have simulated a model polyelectrolyte microgel setup with the corresponding counter ions in a periodic box, using the results mainly to calculate the fraction of counter ions inside the microgel. We compared these results to a Poisson-Boltzmann numerical solution[23,24] in order to see how the mean field solution differs from the results of the simulation. We outlined the differences between these two models, listed as assumptions in section II C, and proceeded to perform a series of simulations aimed at removing these assumptions in a step-wise fashion in order to isolate the effects of each assumption.

The very first assumption of going from a charged sphere with uniform distribution in the PB solver to having discrete charges showed a slight decrease in the fraction of counter ions inside the microgel. The fact that the sucessive "smearing out" of the discrete charges, thus approacing the uniform charge distribution in the PB solver, resluted in a sucessive approach of the LS results to that of the PB calculation shows that the discretization of charges causes the slight decrease of the fraction of counter ions inside the microgel. A further decrease is shown when going from the lattice sphere with evenly spaced charge distribution within the sphere to the static microgel configuration, where the charges are not as evenly distributed since they were lined up within the polymer. Aside from the discretization of charges, the density of charges of the microgel particles also plays a role in fraction of counter ions in the microgel, the two being directly proportional.

Even with the many assumptions in between the MG simulations and PB theory, we have seen that the results of the two methods are quite close to one another. We can therefore safely assume that if PB models with configurations that follow the more complex

configurations found in molecular simulations of real systems are constructed, the results in terms of counter ion condensation from both approaches would be comparatively close, as long as we stick the the basic assumptions used in this study such as movable charges and counter ions, good solvent, and relatively isolated systems. This allows one to use the PB cell model to predict structural or thermodynamic properties of microgels in solution.

Acknowledgments

---

[1] T. R. Hoare and D. S. Kohane, Polymer **49**, 1993 (2008).

[2] A. Richter, G. Paschew, S. Klatt, J. Lienig, K.-F. Arndt, and H.-J. P. Adler, Sensors **8**, 561 (2008).

[3] R. R. N. Netz and D. Andelman, Phys. Rep. **380**, 1 (2003).

[4] J. K. Oh, R. Drumright, D. J. Siegwart, and K. Matyjaszewski, Prog. Polym. Sci. **33**, 448 (2008).

[5] L. Klouda and A. G. Mikos, European Journal of Pharmaceutics and Biopharmaceutics **68**, 34 (2008).

[6] S. Charerji, I. K. Kwon, and K. Park, Prog. Polym. Sci. **32**, 1083 (2007).

[7] B. Baroli, Journal of Pharmaceutical Sciences **96**, 2197 (2007).

[8] J.-L. Barrat and J.-F. Joanny, Adv. Chem. Phys. **94**, 1 (1996).

[9] C. Holm, J.-F. Joanny, K. Kremer, R. R. Netz, P. Reineker, C. Seidel, T. A. Vilgis, and R. G. Winkler, Adv. Polym. Sci. **166**, 67 (2004).

[10] B. A. Mann, R. Everaers, C. Holm, and K. Kremer, Europhys. Lett. **67**, 786 (2004).

[11] H. Schiessel and P. Pincus, Macromolecules **31**, 7953 (1998).

[12] H. Schiessel, Macromolecules **32**, 5673 (1999).

[13] B. A. Mann, C. Holm, and K. Kremer, J. Chem. Phys. **122**, 154903 (2005).

[14] Q. Yan and J. J. de Pablo, Phys. Rev. Lett. **91**, 018301 (2003).

[15] S. Schneider and P. Linse, Eur. Phys. J. E **8**, 457 (2002).

[16] H.-J. Limbach, A. Arnold, B. A. Mann, and C. Holm, Comput. Phys. Commun. **174**, 704 (2006).

[17] G. S. Grest and K. Kremer, Phys. Rev. A **33**, 3628 (1986).

[18] K. Kremer and G. S. Grest, The Journal of Chemical Physics **92**, 5057 (1990).

[19] J. D. Weeks, D. Chandler, and H. C. Andersen, The Journal of Chemical Physics **54**, 5237 (1971).

[20] M. Deserno and C. Holm, The Journal of Chemical Physics **109**, 7678 (1998).

[21] M. Deserno and C. Holm, The Journal of Chemical Physics **109**, 7694 (1998).

[22] A. Katchalsky, Pure and Applied Chemistry **26**, 327 (1971).

[23] M. Deserno, Eur. Phys. J. E **6**, 163 (2001).

[24] M. C. Barbosa, M. Deserno, C. Holm, and R. Messina, Phys. Rev. E **69**, 051401 (2004).

[25] M. Rubenstein and R. H. Colby, *Polymer Physics* (Oxford University Press, New York, USA, 2003).

TABLE I: Parameters common to all simulations in this paper. These are: Lattice Sphere(**C-LS**), Static Microgel (**C-ST**), Microgel in a Spherical Cell (**C-MG**), and Microgel in a Periodic Box (**P-MG**).

Parameter	value
$k_B T$	1.0
ϵ_{LJ}	1.0
l_B	1.0
unit mass m	1.0
time step	0.012
ensemble	NVT
thermostat	Langevin
friction coefficient (Γ)	1.0
time steps for every snapshot	1000
minimum number of snapshots for results	15000
program used	ESPResSo

TABLE II: Simulation parameters for the calculations discussed in sections III B and IV B. The following parameters are common for all these calculations: the radius of the inner sphere $r_0 = 18\sigma$ whose total charge is $q_{sp} = +250.0$, the total number of counter ions is $n_{CI} = 250$, the charge for each coutner ion is $q_{CI} = -1.0$, each counter ion is treated as a point particle with no σ_{LJ} interaction between them, all use the cell model and the electrostatic interactions are calculated via direct sum, the outer radius of the cell is $R = 52\sigma$. The entries left blank in this table are parameters that are not applicable to the specific computation.

Simulation label	PB-1	C-LS-1	C-LS-2	C-LS-3	C-LS-4	C-LS-5	C-ST-1	C-ST-2
number of charged particles (CP)		250	484	894	484	894	250	250
number of uncharged particles		0	0	0	0	0	9	239
excluded volume (σ_{LJ}) of CP		1.0	0.516	0.279	0.802	0.654	1.0	1.0
charge of particle (q_{CP})		1.0	0.516	0.279	0.516	0.279	1.0	1.0
percentage CI in microgel/sphere	52.83	49.80	53.85	52.78	53.36	52.21	46.28	45.67
error of percentage CI		2.01	1.99	2.00	2.00	1.98	2.12	2.09

TABLE III: Simulation parameters for the calculations discussed in section V B. The following parameters are common for all these calculations: the total charge of each particle in the inner sphere is $q_{sp} = +250.0$, the total number of counter ions is $n_{CI} = 250$, the charge of each counter ion is $q_{CI} = -1.0$, the electrostatics of **C-MG** was calculated via direct sum, while the electrostatics of **P-MG** calculation which uses periodic boundary conditions was calculated using P3M. The entries left blank in this table are parameters and results that are not applicable to the specific computation.

Simulation label	**PB-2**	**C-MG**	**P-MG**
radius of sphere r_0 (constant)	14.96		
boundary (Cell or Periodic box)	cell	cell	box
box length L (in σ)			84
outer radius R (in σ)	52	52	
number of charged particles (CP)		250	250
number of uncharged particles		239	239
excluded volume (σ_{LJ}) of CP		1.0	1.0
charge of particle (q_{CP})		1.0	1.0
excluded volume of (σ_{LJ}) of CI			1.0
average squared radius of gyration R_g^2		134.27	134.76
error in R_g^2		4.62	4.51
radius of microgel (eqn. 10)		14.96	14.99
percentage CI in microgel/sphere	55.59	54.03	53.95
error in percentage CI		2.36	2.32

Figure 1. Snapshot of a microgel **P-MG** simulation (shown in perspective) in a periodic box. Figure a. shows how the starting structure was constructed, while figure b. shows one equilibrated structure. The microgel is composed of 46 polymers, each composed of 10 monomers (represented as grey shaded beads). The polymer also contains an additional 29 beads acting as crosslinks (represented as dark beads, larger radius is done only for emphasis), which connect the ends of either three or four polymers. Thus the microgel has a total of 489 beads. Half of the monomers and 20 crosslinks, totalling 250 beads, have a +1.0 charge, giving a total charge of +250.0. The box contains 250 counter ions (not all shown), each with a charge of -1.0, making the box have an overall neutral charge.

Figure 2. Models discussed in section II C to go from the Poisson-Boltzmann spherical cell model (**PB**) to the microgel simulation (**P-MG**). The dark objects are the particles in the lattice (b) or the monomers in the microgel (c-e), while the lighter colored objects are the counterions that are free to move within the boundaries. The numbers on the arrows indicate the assumptions taken when going from one model to the next, as discussed in section II C. a. Poisson-Boltzann spherical cell model (**PB**). b. Lattice sphere (**C-LS**). c. Static microgel (**C-ST**). d. Cell microgel (**C-MG**). e. Microgel (**P-MG**).

Figure 3. Integrated ion probability of simulations listed in Tables II and III, also corresponding to the counter ion densities in figure 4. The inset is a magnification of the regions around $r_0 = 18$ (radius corresponding to table II) and around $r_0 = 14.99$ (radius corresponding to table III). The dots in the inset indicate the numbers reported at the last line in Tables II and III.

Figure 4. Counter ion densities of the simulations listed in Tables II and III, also corresponding to the integrated counter ion probabilities in figure 3. The counter ion density graph of **C-LS-4** is very simlar to **C-LS-2**, that of **C-LS-5** to **C-LS-3**, that of **C-ST-2** to **C-ST-1**, and that of **C-MG** to **P-MG**. These are therefore not included in this figure.

Figure 5. Arrangement of Excluded Volume. Solid circles represent the charged particles, open circles the counter ions, the grey shaded circle represents an uncharged particle, and the dashed circles the excluded volume σ_{LJ} between the particles and the counter ions. a. Lattice sphere **C-LS-1**. The charged particles are at a distance of 4.81 apart for the **C-LS-1**

case, 3.67 for the **C-LS-2** case, and 3.04 for the **C-LS-3** case. After subtracting the two excluded volume radii from the charged particle, the distance x is still greater than Bjerrum length l_B, thus allowing the counter ion to move freely around the dashed circle. b. Static microgel **C-ST-1** without uncharged particles. Since the distance between charged particles is only around 2.0, there is no extra space for the counter ions to freely move once the excluded volume has been taken into account. c. Static microgel **C-ST-2** with uncharged particles in between. The decrease in free space in b and c results in the lowering of the counter ion fraction for the ST case as compared to the LS.
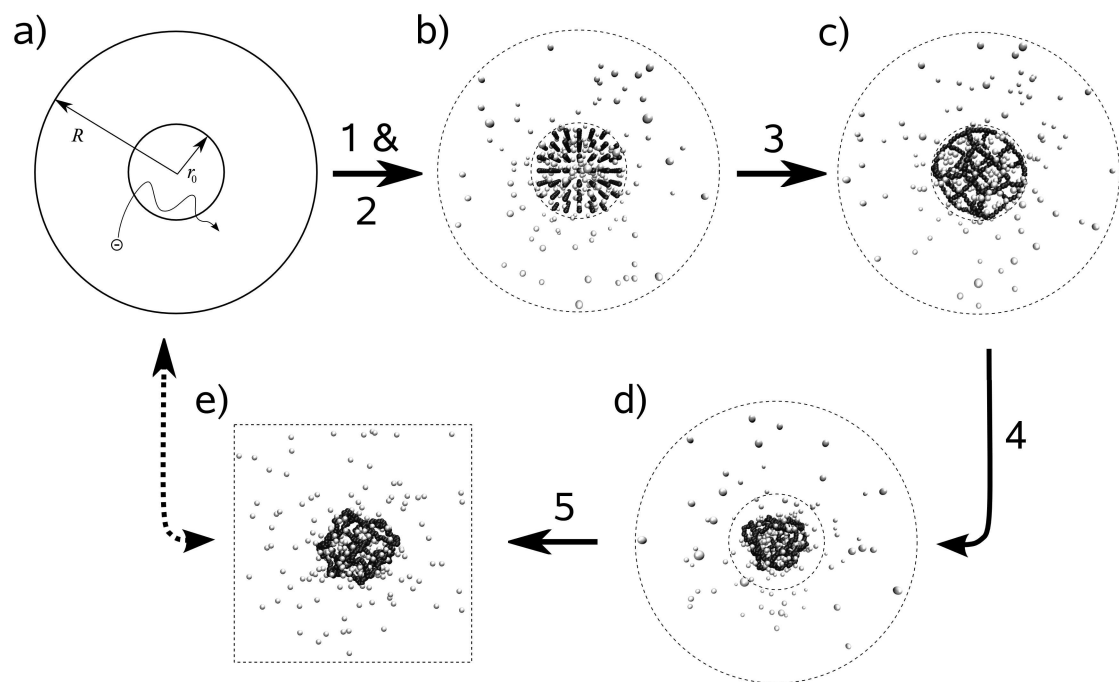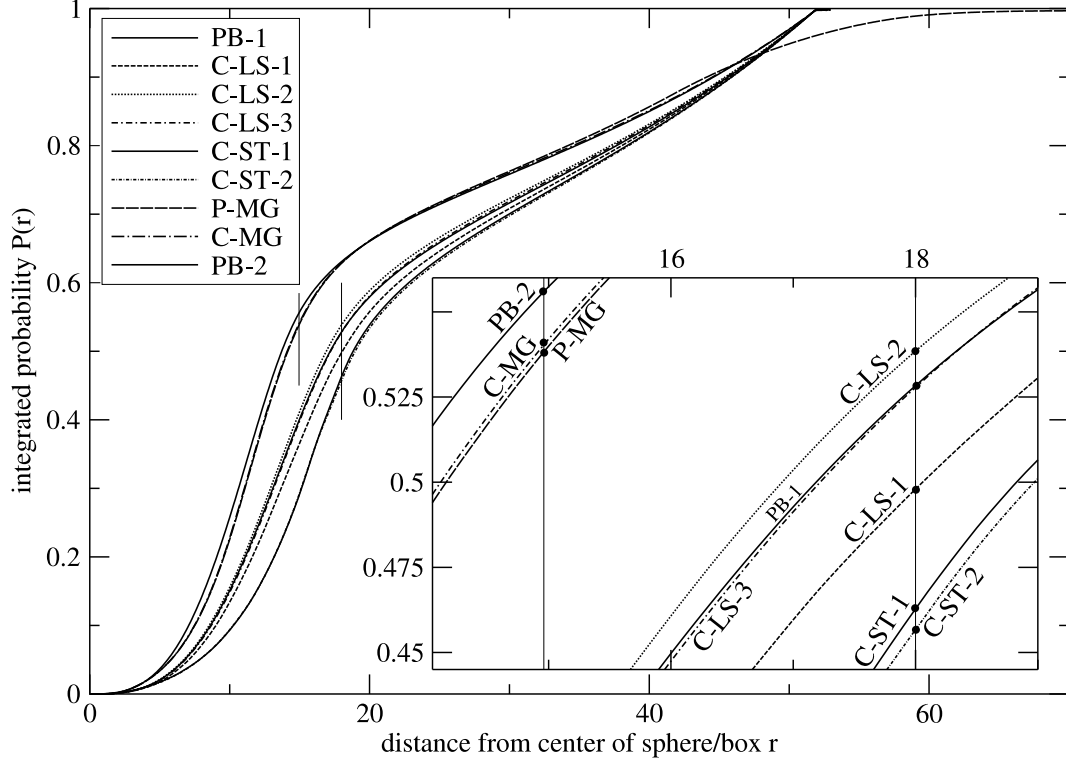
a)

b)

FIG. 1:

FIG. 2:

FIG. 3:

FIG. 4:

a) C-LS-1

b) C-ST-1

c) C-ST-2

FIG. 5: